Desalination and Water Treatment
www.deswater.com

doi: 10.1080/19443994.2016.1148639

57 (2016) 25216–25225
November

Taylor & Francis
Taylor & Francis Group

Adsorption behavior of methylene blue on Fe_3O_4-embedded hybrid magnetic metal–organic framework

Yan Xu[a,*], Jingjie Jin[a], Xianliang Li[b,*], Chaosheng Song[a], Hao Meng[a], Xia Zhang[a,*]

[a]*Department of Chemistry, College of Science, Northeastern University, Shenyang, Liaoning 110819, China, Tel./Fax: +86 024 83684533; emails: xuyanjlu@126.com (Y. Xu), 1725946606@qq.com (J. Jin), 978042006@qq.com (C. Song), 3796477@qq.com (H. Meng), xzhang@mail.neu.edu.cn (X. Zhang)*

[b]*College of Materials Science and Engineering, Shenyang University of Chemical Technology, Shenyang, Liaoning 110142, China, Tel./Fax: +86 024 83684533; email: lixianliang007@163.com*

Received 30 October 2015; Accepted 25 January 2016

ABSTRACT

A magnetic hybrid material (Fe_3O_4-embedded-MOF) consisting of a stable metal–organic framework HKUST-1 embedded with poly(N-vinyl-2-pyrrolidone) coated Fe_3O_4 microspheres was simply prepared under refluxing conditions for 4 h. The as-synthesized material was characterized using powder X-ray diffraction, scanning electron microscopy (SEM), vibrating sample magnetometry (VSM), energy dispersive spectroscopy (EDS) and N_2 adsorption–desorption at 77 K. The hybrid material was studied for the adsorption of methylene blue from aqueous solution. The effects of dye concentration, adsorbent dose, and initial pH on the adsorption of methylene blue were measured, and from these experimental data, adsorption isotherms, kinetics, and thermodynamics were obtained. The results showed that a pseudo-second-order kinetic model and Langmuir isotherm (with $R^2 = 0.937$) matched well for the adsorption of methylene blue onto Fe_3O_4-embedded-MOF. Thermodynamic parameters including free energy, enthalpy, and entropy of methylene blue adsorption were calculated, and the results showed that the adsorption of methylene blue were favorable on Fe_3O_4-embedded-MOF. The magnetic hybrid Fe_3O_4-embedded-MOF material features both magnetic separation characteristics as well as excellent adsorption performance for methylene blue in aqueous solution. The results of the present study demonstrate that Fe_3O_4-embedded-MOF is a promising adsorbent for the removal of dye from wastewater.

Keywords: Hybrid material; Adsorption; Magnetic separation; Kinetics; Isotherm; Thermodynamics

1. Introduction

The increasing contamination of organic dyes in wastewater has promoted researchers to explore more efficient methods for their treatment due to their adverse effects to many forms of life [1,2]. Methylene Blue (MB) is one of the most common dyeing materials from wastewaters of textile, paper, printing, and other industries. The release of the MB contaminant into the environment has posed a significant threat to the environment due to its toxic, carcinogenic, mutagenic, and tetratogenic effects [2].

*Corresponding authors.

Various technologies have been developed for the treatment of dyestuffs, however, due to the stability of dyes to light, heat, and oxidizing agents, adsorption technology is regarded as one of the most competitive methods [3–6]. The common adsorbents include activated carbon, clay, zeolites, red mud, and nanoparticles. Biosorbents are widely studied to remove pollutants from effluents [7–10]. Many researchers are giving considerable attention to the use of agricultural-based biomasses such as corncobs, sugarcane bagasse, cotton sticks, sunflower, and peanut husk as the biosorbent for the removal of dyes from different wastewaters because the agricultural byproducts are cheap and easily obtainable [11–18].

Adsorption using porous materials is also being considered as a possible alternative. Metal–organic frameworks (MOFs) are an emerging class of crystalline materials formed via the coordination chemistry between metal-ion or metal-cluster nodes and multitopic organic linkers [19]. Owing to their tunable pore sizes, large surface areas, and varying structure functionalities, MOFs hold great promise in a wide variety of potential applications [20–22], especially, in separation science. MOFs have become a focus of research concerning environmental purification [22]. For example, Jhung and co-workers grafted protonated ethylenediamine onto Cr-MIL-101 to produce sorbents, which exhibited high adsorption capacity and rapid uptake for the removal of the dye methyl orange (MO) [23]. Wang et al. prepared various polyoxometalates (POMs)-immobilized MIL-100 porous composites, which featured a superior adsorption capacity for MB molecules than the isolated MIL-100 framework, and possessed high selectivity to capture MB from mixtures of MB and MO [24]. However, the separation of these sorbents from wastewater hinders their application. One possible solution is to use magnetic separation as a technique to separate MOF-based sorbents from wastewater by applying an external magnetic field [25]. Thus, it is desirable to develop simple and efficient synthetic methodologies to fabricate new magnetic MOF-based hybrid materials.

To date, several methods have been developed to synthesize magnetic MOF materials. For example, single core-shell magnetic zeolitic imidazolate framework-8 (ZIF-8) using Fe_3O_4 as a core is obtained by controlling heterogeneous growth of ZIF-8 on magnetic Fe_3O_4 nanoparticles through a versatile layer-by-layer strategy. The as-prepared hybrid ZIF-8-based nanocomposites can be used for the enrichment and direct detection of small molecules [26]. Another kind of magnetic hybrid MOF-type material is prepared through the decoration of Fe_3O_4/SiO_2 core-shell magnetic particles on the surface of a MOF via a chemical bonding approach, which possesses desired chemical uniformity and permanent magnetism [27].

Here, we performed a fast and simple strategy to fabricate magnetic PVP-coated Fe_3O_4 microspheres within a HKUST-1 MOF material. The hybrid Fe_3O_4-embedded-MOF material not only exhibits high surface area, large pores, and excellent chemical stability, but also shows obvious adsorption performance toward the MB dye. The adsorption capacity and the factors influencing adsorption such as dye concentration, adsorbent dose, and initial solution pH value, as well as the adsorption isotherms, kinetics, and thermodynamics for the adsorption of MB in aqueous solution were analyzed in detail.

2. Materials and methods

The analytical reagents include ferric trichloride hexahydrate ($FeCl_3{\cdot}6H_2O$, Guangfu, Tianjin, China), sodium citrate ($C_6H_5O_7Na_3{\cdot}H_2O$, Yongda, Tianjin, China), urea (Yongda, Tianjin, China), and polyacrylamide (PAM, Guoyao, Shanghai, China, http://www.sinoreagent.com) were used to prepare magnetic Fe_3O_4 microparticles. Cooper (II) nitrate trihydrate ($Cu(NO_3)_2{\cdot}3H_2O$, Damao, Tianjin, China), 1,3,5-benzenetricarboxylic acid (H_3BTC, Aladdin, Shanghai, China, http://www.aladdin-e.com), N,N-dimethylformamide (DMF, Bodi, Tianjin, China), ethanol (Yongda, Tianjin, China), H_2O ("Wahaha" purified drinking water, China), Methylene Blue (MB, Aladdin, Shanghai, China), and poly(N-vinyl-2-pyrrolidone) (PVP) (PVP, Guoyao, Shanghai, China, http://www.sinoreagent.com). All of the chemical reagents are obtained from commercial sources and used without further purification. An NdFeB permanent magnet (Grade: N35; Coating: Nickel; Diameter: 31 mm; Height: 5 mm, circular-shaped, Tianhe Magnet, Tianjin, China).

2.1. Sample preparations

2.1.1. Preparation of Fe_3O_4 microparticles

Magnetic Fe_3O_4 microparticles were prepared by one-pot hydrothermal method. Briefly, 0.54 g of $FeCl_3$ $6H_2O$ (2 mmol), 1.03 g of sodium citrate ($C_6H_5O_7Na_3$ $2H_2O$) (4 mmol), and 0.36 g of urea (6 mmol) were dissolved in 40 mL pure water. Then 0.3 g of polyacrylamide (PAM) was added under continuous stirring until a clear solution was obtained. The solution was then sealed in a 50 mL Teflon-lined autoclave and heated at 200°C for 12 h. The black precipitation was collected with an extra magnet, washed with pure water and ethanol for several times, and dried overnight at 60°C.

2.1.2. Preparation of Fe_3O_4-embedded-MOF

About 0.05 g of as-prepared Fe_3O_4 microspheres were added to a mixture of PVP (PVP, 0.12 g), 20 mL of pure H_2O, 20 mL of N,N-Dimethylformamide (DMF), and 20 mL of ethanol. Then the mixture was sonicated in a bath-type sonicator for 1 h. An external magnet was attached to the outside of the glass vial to collect the PVP-coated Fe_3O_4 (Fe_3O_4-PVP) microspheres. After the removal of supernatant, the Fe_3O_4–PVP microspheres were dispersed in a mixture of 20 mL pure H_2O, 20 mL N,N-Dimethylformamide (DMF), and 20 mL ethanol, to which 0.5 g of H_3BTC was added and refluxed at 85˚C for 1 h. Then, 1.0 g of $Cu(NO_3)_2$ $3H_2O$ was added to the solution slowly while stirring, and refluxed at 85˚C for another 3 h. After the mixture cooled to room temperature, the generated precipitates (Fe_3O_4-embedded-MOF) were collected by an extra magnet, and dried in a vacuum oven at 60˚C.

2.2. Instrument and characterization

The phase of the samples was characterized by powder X-ray diffraction on a X'Pert Pro MRDDY2094 diffractometer with Cu-Kα radiation (λ = 1.5418 Å). A scan rate of 0.0167 s^{-1} was applied to record the XRD pattern in 2θ range of 6–70˚. The morphology of the samples was observed using Ultra Plus field-emission scanning electron microscope (SEM). The magnetic properties were studied at room temperature by vibrating sample magnetometry (VSM) in the field range from −10,000 to +10,000 Oe. Nitrogen adsorption–desorption isotherms were recorded with a Micromeritics ASAP-2020 M volumetric gas sorption apparatus using 99.999% of pure N_2. The UV–visible adsorption spectra were recorded using a Hitachi U-3,010 UV–visible spectrometer.

2.3. Adsorption experiments

Typically, 15 mg of Fe_3O_4-embedded-MOF was dispersed in 5 mL of MB aqueous solution with a known initial concentration at pH of 7 at room temperature. Then, an external magnet was attached to the outside of the glass vial. After a few seconds, the Fe_3O_4-embedded-MOF composite was gathered to the inner wall of the vial, and the supernatant was removed out to perform analysis. The residual concentration of MB was determined by UV–visible spectrophotometer at the maximum adsorption wavelength of 664 nm. The removal efficiency (%) of dye and the amount of dye uptake per unit of adsorbent (q_e) were calculated [16]. Adsorption experiments were conducted in batches to study the effects of initial MB concentration, adsorbent dose, and initial solution pH value for MB adsorption. Comparing with those biosorbents, the hybrid Fe_3O_4-embedded-MOF here we used made separation faster and easier with an extra magnet, and avoids time-consuming process or filtration operations. The figures of merit of reported biosorbents for the removal of dyestuffs are listed in Table 1.

3. Results and discussion

3.1. Characterization

Fig. 1(a) shows the simulated XRD pattern of MOF HKUST-1 generated based on the reported crystal structure data [28]. Fig. 1(b) and Fig. 1(c) show the experimental XRD patterns of the as-prepared Fe_3O_4, and Fe_3O_4-embedded-MOF samples. The XRD pattern of Fe_3O_4-embedded-MOF is almost identical to the simulated XRD pattern of MOF HKUST-1, indicating that the crystalline structure of HKUST-1 host matrix remains nearly unchanged after the incorporation of Fe_3O_4 microspheres. In addition, no obvious X-ray diffractions from Fe_3O_4 microspheres are observed in Fig. 1(c), which is probably due to the low concentrations of embedded Fe_3O_4 microspheres. Besides, the thick HKUST-1 crystalline coverage may exceed the penetration depth of X-rays, resulting in the missing signals of Fe_3O_4 microspheres in the XRD pattern of Fe_3O_4-embedded-MOF.

The structure, morphology of the as-prepared Fe_3O_4, and Fe_3O_4-embedded-MOF samples were characterized by SEM. As shown in Fig. 2(a), the obtained Fe_3O_4 microspheres possess narrow size distribution, and the overall mean diameter of Fe_3O_4 microspheres is about 185 nm. Fig. 2(b) shows the block morphology of Fe_3O_4-embedded-MOF hybrid material, the size of which is about 7–15 μm in diameter. Fig. 2(c) shows the field-dependent magnetization curve of the Fe_3O_4-embedded-MOF hybrid material at room temperature. The saturation magnetization value for Fe_3O_4-embedded-MOF is 2.8 emu g^{-1}, which is large enough for magnetic separation. The EDS result shown in Fig. 2(d) also demonstrates the existence of iron in the large crystal of the final hybrid material. Nitrogen adsorption was performed to investigate the pore properties of pure MOF HKUST-1 and Fe_3O_4-embedded-MOF. The isotherm curves of MOF HKUST-1 and Fe_3O_4-embedded-MOF are shown in Fig. 3. The BET surface areas for MOF HKUST-1 and Fe_3O_4-embedded-MOF were calculated to be 1,316 and 939 m^2 g^{-1}, with pore volume of 0.59 and 0.44 cm^3 g^{-1}, respectively.

Table 1
Figures of merit of reported biosorbents for dyestuffs treatment

Materials	Removal efficiency	Optimum pH	Adsorption capacity (mg g^{-1})	Interferences	Refs.
Sugarcane bagasse	–	2	65.8 mg g^{-1} (Direct Yellow 50 dye)	A: pH B: Contact time C: Biosorbent dose D: Initial dye concentration E: Temperature	[11]
Corncobs	79% (Textile wasterwater)	2	–	A: Biosorbent dose B: Shaking speed C: Temperature	[12]
Polyethyleneimmine-treated sugarcane bagasse	–	2	19.54 mg g^{-1} (Novacron Orange P-2R)	A: Modifications/ Treatments B: pH C: Biosorbent dose D: Initial dye concentration E: Contact time F: Temperature	[13]
Hen feather	95.2% (Bismark Brown R) >70% (Brilliant Blue FCF) ~85% (Malachite Green)	3, 2, and 7, respectively	–	A: Adsorbent dose B: Dye concentration C: pH D: Contact time E: Temperature	[14–16]
Polyethyleneimmine-treated peanut husk	–	Acidic	141 and 98.2 mg g^{-1} (Indosol Black NF and Indosol Orange RSN)	A: Initial dye concentration B: Biosorbent dose C: pH	[17]
Peanut hulls	–	2	–	A: pH B: Biosorbent dose C: Initial dye concentration D: Contact time E: Temperature	[18]
Fe_3O_4-embedded-MOF	~70% (Methylene Blue)	7	–	A: Initial dye concentration B: Adsorbent dose C: pH D: Contact time	This work

3.2. Effect of initial MB concentration

About 15 mg of Fe_3O_4-embedded-MOF was used in the adsorption experiment and dispersed into 5 mL of MB solution with different concentrations (5, 10, 14, and 18 mg L^{-1}). The experiments were performed at pH of 7 at room temperature. As shown in Fig. 4(a), the maximum adsorption capacity for Fe_3O_4-embedded-MOF are 1.53, 2.86, 2.84, and 2.96 mg g^{-1}, with MB concentrations of 5, 10, 14, and 18 mg L^{-1}, respectively, and the adsorption reaches equilibrium after about 15 min. In addition, it is found that the adsorption capacity (q_e) does not change very much with increasing initial MB concentration from 10 to 18 mg L^{-1}.

3.3. Effect of adsorbent dose

Fig. 4(b) shows the effect of adsorbent dose (2–6 g L^{-1}) on removal efficiency of MB (12 mg L^{-1}) at pH of 7 when the equilibrium was reached. As shown in Fig. 4(b), the removal efficiency increases with the increasing adsorbent dose, probably due to the greater adsorbent surface area and pore volume available at higher adsorbent dose providing more active adsorption sites that result in a higher removable efficiency, however, the MB adsorbed by per unit adsorbent at equilibrium (q_e mg g^{-1}) decreases with the increasing adsorbent dose from 2 g L^{-1} (10 mg per 5 mL of dye solution) to 6 g L^{-1} (30 mg per 5 mL of dye solution),

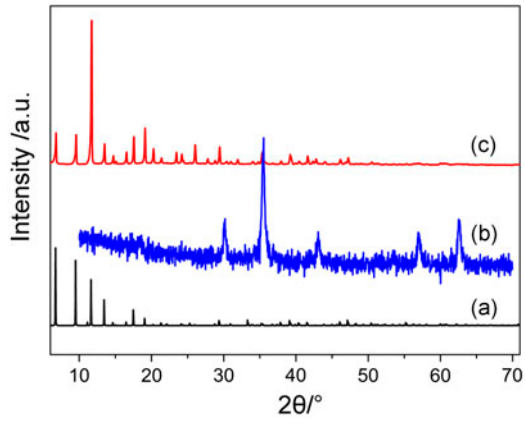

Fig. 1. (a) The stimulated XRD pattern derived from single crystal of MOF HKUST-1, (b) as-prepared Fe_3O_4, and (c) Fe_3O_4-embedded-MOF samples.

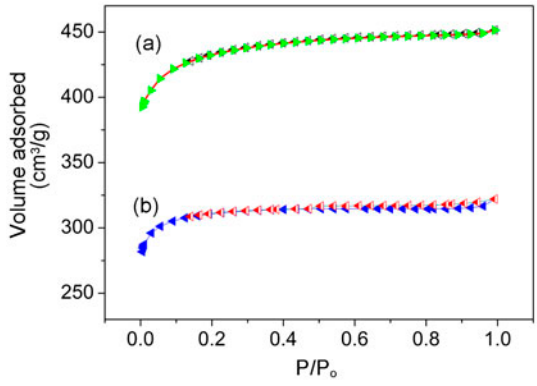

Fig. 3. N_2 adsorption–desorption isotherms of (a) MOF HKUST-1 and (b) Fe_3O_4-embedded-MOF.

so 3 g L^{-1} (15 mg per 5 mL of dye solution) was selected in the following investigation of adsorption isotherm, kinetics, and thermodynamics experiments.

3.4. Effect of initial solution pH

To study the effect of pH on the removal of MB from aqueous solution, 15 mg of Fe_3O_4-embedded-MOF was used as an adsorbent and dispersed in 5 mL of MB aqueous solution (8 mg L^{-1}). The initial pH of the solution before the adsorbent experiment was adjusted with 0.1 mol L^{-1} HCl and 0.5 mol L^{-1} NaOH solutions. Ultraviolet absorption spectroscopy was used to determine the concentration of MB solution.

As shown in Fig. 4(c), according to the pH effect on the zeta potential of MOF HKUST-1, the surface charge of HKUST-1 is neganive for pH ≥ 5, and the MB usually exists as a positive cation [29]. Thus, high

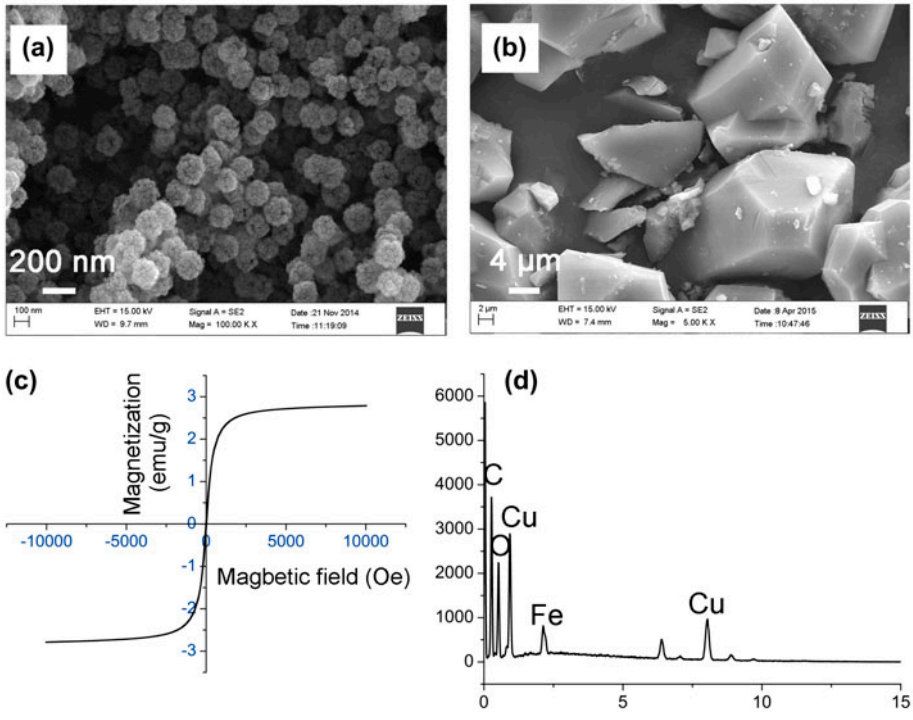

Fig. 2. SEM images of (a) as-prepared Fe_3O_4, (b) Fe_3O_4-embedded-MOF, (c) magnetization curves, and (d) EDS spectrum of Fe_3O_4-embedded-MOF.

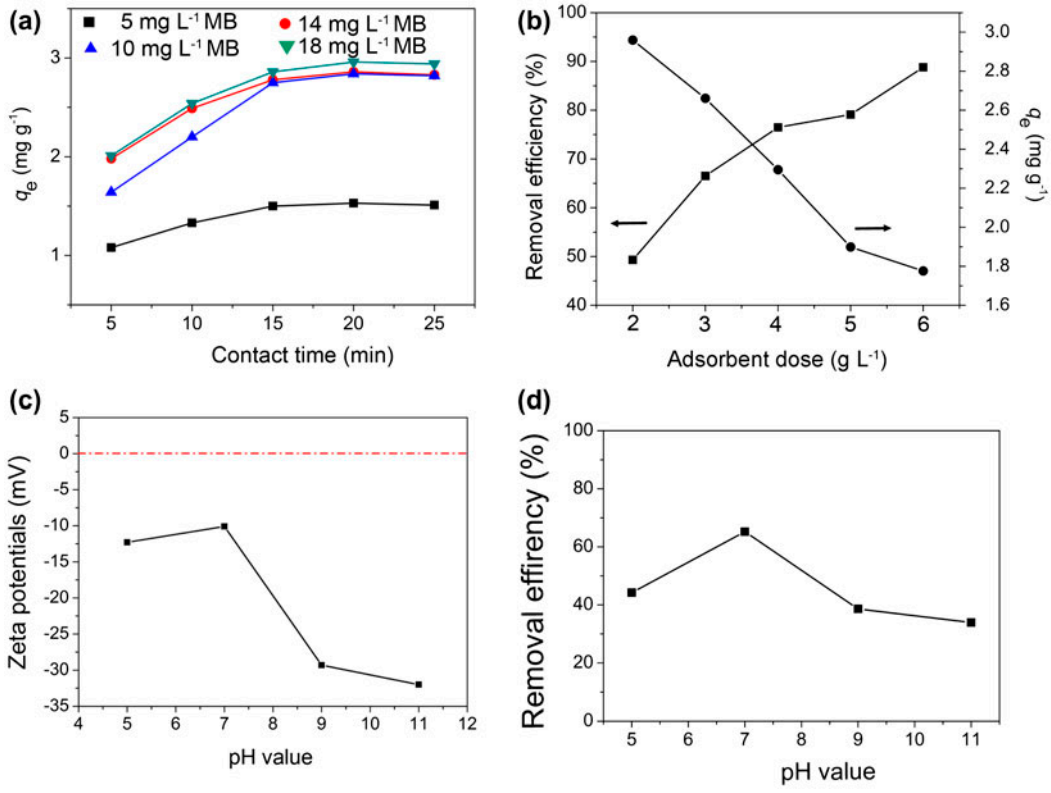

Fig. 4. (a) Effects of initial MB concentration, (b) adsorbent dose for the adsorption of MB, (c) the pH effect on the zeta potential of Fe_3O_4-embedded-MOF, and (d) effect of initial solution pH for the adsorption of MB.

electrostatic interaction between the negative surface charge of Fe_3O_4-embedded-MOF and positive MB dye will favor adsorption. The equilibrium MB removal efficiency increased with increasing pH from 5 to 7 (Fig. 4(d)), because more H^+ at lower pH might compete with MB dye cations, causing decrease in the amount of dye adsorbed. As the pH value increased from 7 to 11, the adsorption of MB decreased due to the reaction between MB-S^+Cl (aq) and NaOH to produce MB-S^+OH (aq) and NaCl (aq). The NaCl salt might reduce the adsorption of MB-S^+OH (aq) on Fe_3O_4-embedded-MOF. The maximum removal efficiency was reached at pH 7. Therefore, the adsorption of MB on Fe_3O_4-embedded-MOF was performed at pH 7 in the following adsorption isotherm, kinetics, and thermodynamics experiments.

3.5. Adsorption isotherm

The adsorption isotherm indicates how the adsorbed molecules distribute between the liquid and solid phase when the adsorption process reaches equilibrium. Three commonly used models (the Freundlich [30], Langmuir [31], and Temkin isotherms [32]) were selected to study the adsorption isotherm. The linear forms of Freundlich, Langmuir, and Temkin equations are given in Eqs. (1)–(3):

$$\ln q_e = \ln K_F + \frac{1}{n} \ln C_e \tag{1}$$

$$\frac{1}{q_e} = \frac{1}{K_L q_L} \frac{1}{C_e} + \frac{1}{q_L} \tag{2}$$

$$q_e = \frac{RT}{b_T} \ln K_T + \frac{RT}{b_T} \ln C_e \tag{3}$$

where q_e (mg g^{-1}) is the amount of dye adsorbed per unit adsorbent at equilibrium, C_e (mg L^{-1}) is the equilibrium concentration of the dye solution, K_F and n are Freundlich adsorption isotherm constants, indicative of the adsorption capacity of the adsorbent and favorableness of the adsorption process, respectively. K_L is the Langmuir constant related to the rate of adsorption, and q_L (mg g^{-1}) is the Langmuir maximum uptake of MB per unit mass adsorbent. R is the common gas constant (8.314 J^{-1} mol^{-1} K^{-1}), T is the absolute temperature (K), b_T and K_T are Temkin

Table 2
Isotherm parameters for MB adsorption on magnetic Fe_3O_4-embedded-MOF material

		Freundlich			Langmuir			Temkin		
Initial MB (mg L^{-1})	$q_{e(exp)}$ (mg g^{-1})	K_F	$1/n$	R^2	K_L	q_L (mg g^{-1})	R^2	b_T	K_T	R^2
5	1.53	2.08	0.761	0.608	2.21	3.27	0.937	5.84	172.6	0.629
10	2.86									
14	2.84									
18	2.96									

constants related to the adsorption potential and adsorption capacity, respectively.

The fitting results and calculated constants for the three isotherm models along with R^2 values are presented in Table 2 and Fig. 5. The results show that the Langmuir isotherm gives the best fittings with $R^2 = 0.937$, which is superior to the Freundlich model and Temkin model, indicating a monolayer adsorption of MB on the surface of magnetic hybrid Fe_3O_4-embedded-MOF material.

3.6. Adsorption kinetics

In order to investigate the MB adsorption kinetics on the Fe_3O_4-embedded-MOF, three commonly used models, namely, pseudo-first-order [33], pseudo-second-order [34], and intra-particle diffusion [35] are applied to interpret the absorption dynamics. These models can be expressed as Eqs. (4)–(6):

$$\text{Pseudo-first order model}: \ln(q_e - q_t) = \ln q_e - k_1 t \quad (4)$$

$$\text{Pseudo-second order model}: \frac{t}{q_t} = \frac{1}{k_2 q_e^2} + \frac{t}{q_e} \quad (5)$$

$$\text{Intra-particle diffusion model}: q_t = k_3 t^{1/2} + C \quad (6)$$

where q_e and q_t (mg g^{-1}) are the uptake of dye per unit of adsorbent at equilibrium, respectively, at time t

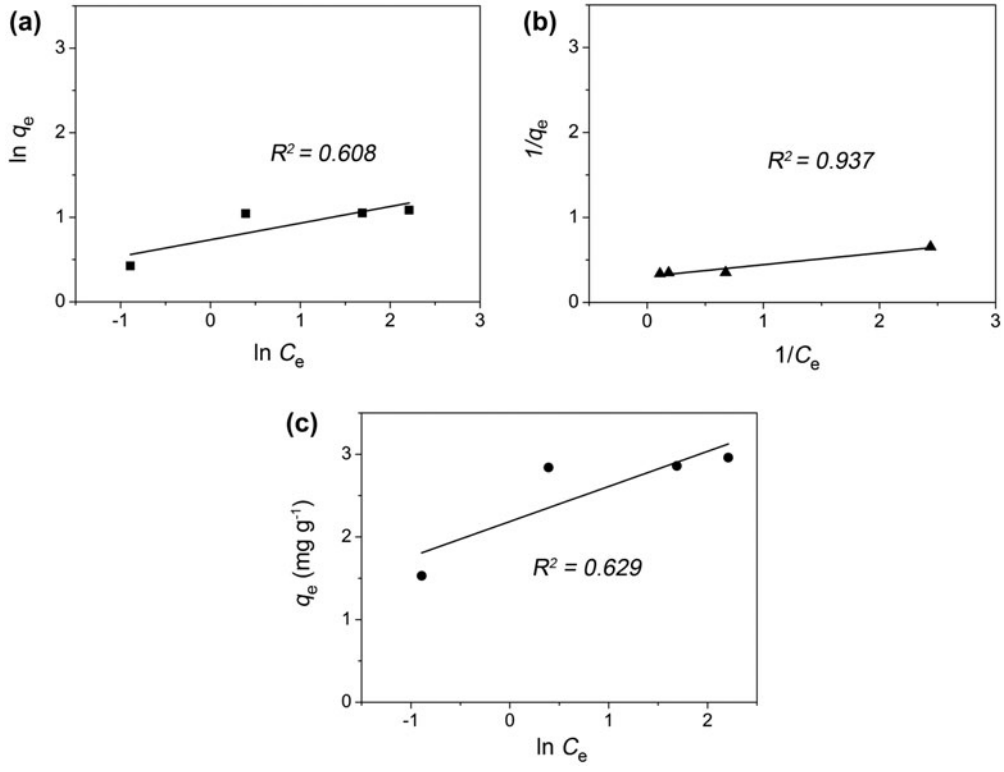

Fig. 5. Linear isotherm plots of (a) Freundlich, (b) Langmuir, and (c) Temkin isotherm for the adsorption of MB on Fe_3O_4-embedded-MOF.

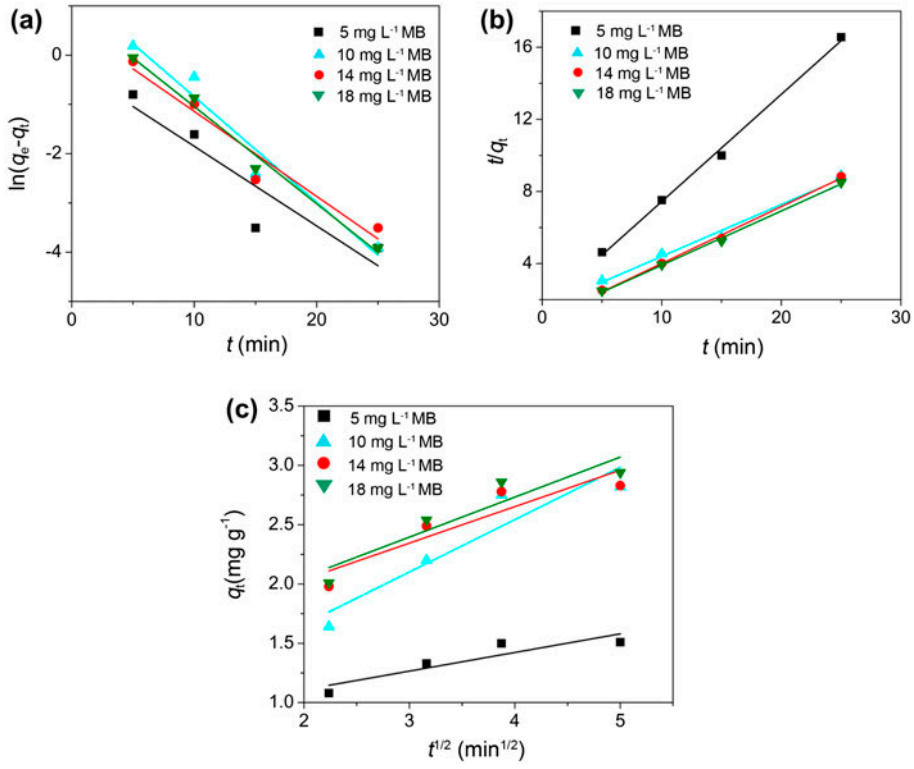

Fig. 6. The fitting lines of (a) pseudo-first-order, (b) pseudo-second-order, and (c) intra-particle diffusion adsorption kinetics for the adsorption of MB on Fe_3O_4-embedded-MOF.

Table 3
Kinetic parameters for MB adsorption on Fe_3O_4-embedded-MOF material

		Pseudo-first-order			Pseudo-second-order			Intra-particle diffusion model		
Initial MB (mg L^{-1})	$q_{e,exp}$ (mg g^{-1})	$q_{e1,cal}$ (mg g^{-1})	k_1 (min^{-1})	R^2	$q_{e2,cal}$ (mg g^{-1})	k_2 (g mg^{-1} min^{-1})	R^2	C (mg g^{-1})	k_3 (g mg^{-1} $min^{1/2}$)	R^2
5	1.53	0.79	0.1617	0.783	1.68	0.2354	0.995	0.7934	0.1574	0.751
10	2.86	3.69	0.2146	0.939	3.48	0.0539	0.984	0.7780	0.4413	0.814
14	2.84	1.79	0.1726	0.920	2.81	0.1472	0.996	1.4235	0.3073	0.768
18	2.96	2.54	0.1974	0.980	3.33	0.0986	0.997	1.3846	0.3372	0.803

(min). k_1 (min^{-1}) and k_2 (g mg^{-1} min^{-1}) are the rate constants of the pseudo-first-order and pseudo-second-order equation, and k_3 (mg g^{-1} $min^{-1/2}$) is the intra-particle diffusion rate constant.

The fitting results for the MB adsorption using the three kinetic models according to Eqs. (6)–(8) are shown in Fig. 6. The kinetic parameters of the three kinetic models are shown in Table 3. Compared to pseudo-first-order ($R^2 < 0.98$) and intra-particle diffusion kinetic model ($R^2 < 0.82$), the pseudo-second order correctly described the kinetic of MB adsorption with $R^2 > 0.98$.

3.7. Thermodynamic study

Thermodynamic study on the MB adsorption was examined by varying the adsorption temperature at 310, 317, 324, and 338 K by adjusting the temperature controller of the water bath sonicator. The enthalpy (ΔH) and the entropy (ΔS) parameters for MB adsorption can be calculated from the intercept and slope of the plot of ln K_c vs. $1/T$ according to Eqs. (7)–(8):

$$\Delta G = -RT \ln K_C \quad (7)$$

$$\ln K_C = -\frac{\Delta H}{R}\frac{1}{T} + \frac{\Delta S}{R} \quad (8)$$

where K_C is the ratio of the equilibrium concentration of the dye ions on adsorbent to that in solution. R is the ideal gas constant (8.314 J mol^{-1} K^{-1}) and T is the adsorption temperature in Kelvin.

Plot of $\ln K_C$ vs. $1/T$ is used to calculate the thermodynamic parameters of ΔH, ΔS, and ΔG for the adsorption of MB by the Fe_3O_4-embedded-MOF at different temperature. The value of ΔH (36.48 kJ mol^{-1}) is positive, which revealed that the adsorption is endothermic. The positive value of ΔS (121.69 J mol K^{-1}) indicates an increase in the randomness at solid–liquid interface during the adsorption. The overall ΔG at 310, 317, 324, and 338 K are −1.24, −2.10, −2.95, and −4.65 kJ mol^{-1}, respectively, indicating a thermodynamically spontaneous nature for the adsorption of MB.

3.8. Adsorption mechanism

As has been mentioned above, the surface of Fe_3O_4-embedded-MOF was negatively charged in the investigated pH range of 5–11, which was beneficial for the adsorption of cationic MB dye through electrostatic forces of attraction. More H^+ at lower pH (5–7) might compete with MB dye cations, causing a little decrease in MB dye adsorption amount. The adsorption of MB also decreased at higher pH between 7 and 11, which is due to the reaction between MB-S$^+$Cl (aq) and NaOH to produce MB-S$^+$OH (aq) and NaCl (aq). The salt of NaCl might decrease the adsorption amount of MB-S$^+$OH (aq) on the Fe_3O_4-embedded-MOF. Besides, the weak interactions including π–π interactions and hydrogen bonds existing between 1,3,5-benzenetricarboxylic acid in HKUST-1 and the MB dye molecules might also contribute to the adsorption efficiency.

4. Conclusions

In summary, magnetic PVP-coated Fe_3O_4 microspheres were successfully embedded into HKUST-1 MOF without losing the crystalline nature of MOF. The as-prepared magnetic hybrid Fe_3O_4-embedded-MOF material exhibits both adsorption properties for MB dye from aqueous solution and magnetic separation characteristics. The adsorption experimental results showed that pseudo-second-order model can be well used to describe the adsorption kinetics. The adsorption isotherms followed a Langmuir isotherm, indicating a monolayer adsorption process. Thermodynamic experimental results demonstrated that the adsorption of MB on Fe_3O_4-embedded-MOF is a thermodynamically spontaneous process.

Acknowledgments

This work was supported by the National Natural Science Foundation of China (grant number 21401018) and the Fundamental Research Funds for the Central Universities (No. N130305003).

References

[1] A. Mittal, Retrospection of bhopal gas tragedy, Toxico. Enviro. Chem. (2015). doi: 10.1080/02772248.2015.1125903.
[2] A. Mittal, J. Mittal, Hen Feather: A remarkable adsorbent for dye removal, in: S.K. Sharma (Ed.), Green Chemistry for Dyes Removal from Wastewater: Research Trends and Applications, John Wiley & Sons, Inc., Hoboken, NJ, 2015, pp. 409–457.
[3] A. Mittal, L. Kurup, Column operations for the removal and recovery of a hazardous dye Acid Red-27 from aqueous solutions, using waste rnaterials-bottom ash and de-oiled soya, Ecol. Environ. Conserv. 12 (2006) 181–186.
[4] M. Naushad, A. Mittal, M. Rathore, V. Gupta, Ion-exchange kinetic studies for Cd(II), Co(II), Cu(II), and Pb (II) metal ions over a composite cation exchanger, Desalin. Water Treat. 54 (2015) 2883–2890.
[5] A. Mittal, R. Ahmad, I. Hasan, Poly (methyl methacrylate)-grafted alginate/Fe_3O_4 nanocomposite: Synthesis and its application for the removal of heavy metal ions, Desal. Wat. Treat. (2015). doi: 10.1080/19443994.2015.1104726.
[6] A. Mittal, M. Naushad, G. Sharma, Z.A. Alothman, S.M. Wabaidur, M. Alam, Fabrication of MWCNTs/ThO_2 nanocomposite and its adsorption behavior for the removal of Pb(II) metal from aqueous medium, Desal. Wat. Treat. (2015). doi: 10.1080/19443994.2015.1125805.
[7] H. Daraei, A. Mittal, M. Noorisepehr, J. Mittal, Separation of chromium from water samples using eggshell powder as a low-cost sorbent: kinetic and thermodynamic studies, Desal. Wat. Treat. 53 (2015) 214–220.
[8] G. Sharma, M. Naushad, D. Pathania, A. Mittal, G.E. EI-desoky, Modification of Hibiscus cannabinus fiber by graft copolymerization: Application for dye removal, Desal. Wat. Treat. 54 (2015) 3114–3121.
[9] A. Mittal, R. Ahmad, I. Hasan, Iron oxide-impregnated dextrin nanocomposite: Synthesis and its application for the biosorption of Cr(VI) ions from aqueous solution, Desal. Wat. Treat. (2015). doi: 10.1080/19443994.2015.1070764.
[10] A. Mittal, R. Ahmad, I. Hasan, Biosorption of Pb^{2+}, Ni^{2+} and Cu^{2+} ions from aqueous solutions by L-cystein-modified montmorillonite-immobilizaed alginate nanocomposite, Desal. Wat. Treat. (2015). doi: 10.1080/19443994.2015.1086900.
[11] S. Sadaf, H.N. Bhatti, S. Nausheen, M. Amin, Application of a novel lignocellulosic biomaterial for the removal of Direct Yellow 50 dye from aqueous solution: Batch and column study, J. Taiwan Inst. Chem. Eng. 47 (2015) 160–170.

[12] H.N. Bhatti, S. Sadaf, A. Aleem, Treatment of textile effluents by low cost agricultural wastes: Batch biosorption study, J. Anim. Plant Sci. 25 (2015) 284–289.
[13] S. Noreen, H.N. Bhatti, Fitting of equilibrium and kinetic data for the removal of Novacron Orange P-2R by sugarcane bagasse, J. Ind. Eng. Chem. 20 (2014) 1684–1692.
[14] J. Mittal, V. Thakur, A. Mittal, Batch removal of hazardous azo dye Bismark Brown R using waste material hen feather, Ecol. Eng. 60 (2013) 249–253.
[15] A. Mittal, Use of hen feathers as potential adsorbent for the removal of a hazardous dye, Brilliant Blue FCF, from wastewater, J. Hazard. Mater. 128 (2006) 233–239.
[16] A. Mittal, Adsorption kinetics of removal of a toxic dye, Malachite Green, from wastewater by using hen feathers, J. Hazard. Mater. 133 (2006) 196–202.
[17] S. Sadaf, H.N. Bhatti, M. Arif, M. Amin, F. Nazar, Adsorptive removal of direct dyes by PEI-treated peanut husk biomass: Box–Behnken experimental design, Chem. Ecol. 31 (2015) 252–264.
[18] S. Noreen, H.N. Bhatti, S. Nausheen, M. Zahid, S. Asim, Biosorption of Drimarine Blue HF-RL using raw, pretreated, and immobilized peanut hulls, Desalin. Water Treat. 52 (2014) 7339–7353.
[19] O.M. Yaghi, M. O'Keeffe, N.W. Ockwig, H.K. Chae, M. Eddaoudi, J. Kim, Reticular synthesis and the design of new materials, Nature 423 (2003) 705–714.
[20] J. Lee, O.K. Farha, J. Roberts, K. Scheidt, S.T. Nguyen, J.T. Hupp, Metal–organic framework materials as catalysts, Chem. Soc. Rev. 38 (2009) 1450–1459.
[21] L.E. Kreno, K. Leong, O.K. Farha, M. Allendorf, R.P. Van Duyne, J.T. Hupp, Metal–organic framework materials as chemical sensors, Chem. Rev. 112 (2012) 1105–1125.
[22] E. Barea, C. Montoro, J.A.R. Navarro, Toxic gas removal–metal–organic frameworks for the capture and degradation of toxic gases and vapours, Chem. Soc. Rev. 43 (2014) 5419–5430.
[23] E. Haque, J.E. Lee, I.T. Jang, Y.K. Hwang, J.S. Chang, J. Jegal, S.H. Jhung, Adsorptive removal of methyl orange from aqueous solution with metal–organic frameworks, porous chromium-benzenedicarboxylates, J. Hazard. Mater. 181 (2010) 535–542.
[24] A.X. Yan, S. Yao, Y.G. Li, Z.M. Zhang, Y. Lu, W.L. Chen, E.B. Wang, Incorporating polyoxometalates into a porous MOF greatly improves its selective adsorption of cationic dyes, Chem. Eur. J. 20 (2014) 6927–6933.
[25] F. Ke, L.G. Qiu, Y.P. Yuan, X. Jiang, J.F. Zhu, Fe_3O_4@-MOF core–shell magnetic microspheres with a designable metal–organic framework shell, J. Hazard. Mater. 22 (2012) 9497–9500.
[26] J. Zheng, C. Cheng, W.J. Fang, C. Chen, R.W. Yan, H.X. Huai, C.C. Wang, Surfactant-free synthesis of a Fe_3O_4@ZIF-8 core–shell heterostructure for adsorption of methylene blue, Cryst. Eng. Commun. 16 (2014) 3960–3964.
[27] Y. Xu, J. Jin, X. Li, Y. Han, H. Meng, T. Wang, X. Zhang, Fabrication of hybrid magnetic HKUST-1 and its highly efficient adsorption performance for Congo red dye, RSC Adv. 5 (2015) 19199–19202.
[28] S.S.Y. Chui, M.F. Lo, J.P.H. Charmant, A.G. Orpen, I.D. Williams, A chemically functionalizable nanoporous material $[Cu_3(TMA)_2(H_2O)_3]_n$, Science 283 (1999) 1148–1150.
[29] S. Eftekhari, A. Habibi-Yangjeh, Sh. Sohrabnezhad, Application of AlMCM-41 for competitive adsorption of methylene blue and rhodamine B: Thermodynamic and kinetic studies, J. Hazard. Mater. 178 (2010) 349–355.
[30] H.M.F. Freundlich, Über die adsorption in lösungen, Z. Phys. Chem. 57 (1906) 385–470.
[31] I. Langmuir, The constitution and fundamental properties of solids and liquids. part I. solids, J. Am. Chem. Soc. 38 (1916) 2221–2295.
[32] M.I. Tempkin, V. Pyzhev, Kinetics of ammonia synthesis on promoted iron catalysts, Acta Phys. Chim. Sin. 12 (1940) 327–356.
[33] V.K. Gupta, A. Mittal, L. Krishnan, V. Gajbe, Adsorption kinetics and column operations for the removal and recovery of malachite green from wastewater using bottom ash, Sep. Purif. Technol. 40 (2004) 87–96.
[34] Y.S. Ho, G. McKay, Pseudo-second order model for sorption processes, Process Biochem. 34 (1999) 451–465.
[35] D. Kavitha, C. Namasivayam, Experimental and kinetic studies on methylene blue adsorption by coir pith carbon, Bioresour. Technol. 98 (2007) 14–21.